Numerical study of eddy generation in the western part of the Gulf of Lion.

Z. Y. Hu,[1,2] A. A. Petrenko,[1] A. M. Doglioli,[1] I. Dekeyser[1]

[1]Aix-Marseille Université; CNRS; IRD;
LOPB-UMR6535, Laboratoire
d'Océanographie Physique et
Biogéochimique, OSU/Centre d'Océanologie
de Marseille, Campus de Luminy case 901,
13288 Marseille Cedex 9, France.

[2]Now at: Key Laboratory of Marine
Ecology and Environmental Science,
Institute of Oceanology, Chinese Academy
of Sciences, 7 Nanhai Road, 266071
Qingdao, China.

Abstract. A realistic numerical model is used to investigate the generation process of anticyclonic eddies located in the western part of the Gulf of Lion. During 8 years of simulations from 2001 to 2008, 8 anticyclonic coastal eddies with a life duration longer than 15 days have been observed in the study area between July and early October. The formation process of eddies is investigated by examining the changes in wind forcing and in stratification conditions. These factors alone or combined are discussed regarding eddy's formation processes. Our results show that these eddies need two conditions to be generated: a persistent and strong northwest wind and a strong stratification. The Ekman transport associated to such a wind and the coastline shape characterized by the presence of capes can create a pressure gradient generating an anticyclonic circulation. At the same time, a strong stratification condition allows a better transfer of wind-induced potential energy to eddy kinetic energy. Persistent wind bursts are also required to sustain the eddy in size and intensity. The present work contributes to a better understanding of the hydrodynamics of the Gulf of Lion.

Keywords: Coastal eddies, regional modeling, mesoscale, Gulf of Lion.

1. Introduction

The Gulf of Lion (hereafter GoL) is a large continental shelf located in the northwestern Mediterranean Sea (Fig. 1). As described by *Millot* [1990], the hydrodynamics of the GoL are complex and highly variable, influenced by three main forcings coexisting in this area:
i) strong continental winds: Tramontane (northwesterly/NW, sometimes westerly) and Mistral (northerly/N). The up- and downwelling phenomena generated by the wind along the coast are well-known [*Millot*, 1979, 1982; *Hua and Thomasset*, 1983];
ii) a mesoscale quasi-geostrophic current, the Northern Current (NC) [*Millot*, 1991], flowing along the GoL continental slope from the Ligurian Sea to the Catalan Sea (Fig. 1). The hydrodynamics of the NC have been well investigated by previous studies [*Millot*, 1990, 1999; *Albérola et al.*, 1995; *Sammari et al.*, 1995; *Petrenko*, 2003; *Flexas et al.*, 2002; *Echevin et al.*, 2003];
iii) fresh water inputs from the Rhône river, bringing nutrients that enhance primary productivity on the shelf [e.g. *Minas and Minas*, 1989; *Ludwig et al.*, 2009]. The river plume extends offshore towards the southwest part of the GoL under certain meteorological conditions [*Estournel et al.*, 1997].

A mesoscale anticyclonic circulation in the western part of the GoL has been first observed by *Millot* [1979, 1982] in the currents and SST images. In the latter, it was partly identified as a tongue of cold water upwelled south of Cape d'Agde. Its signature can also be observed in SeaWiFs chlorophyll maps with a high chlorophyll *a* plume on its northern edge circling around the eddy [*Hu et al.*, 2009]. During the oceanographic cruise Latex08, *Hu et al.* [2011] also observed an anticyclonic eddy in the western part

of the GoL and suggested that the radius of the eddy is estimated to be 15-20 km. The maximum life duration of these anticyclonic eddies is estimated to be up to about 2 months [*Hu et al.*, 2009, 2011]. The spatial and temporal scales of these coastal eddies are distinct from those of the large eddies observed in the open ocean like the Gulf Stream rings and the Agulhas rings. They are also smaller than those of the eddies observed in the Mediterranean sub-basin, such as the Algerian eddies which can have lifetimes up to $\sim$3 years and can reach diameters larger than $\sim$250 km [*Millot*, 2003; *Ruiz et al.*, 2002]. However, eddies are among the physical processes that can have an important role over the continental shelf edge listed by [*Huthnance*, 1995]. Indeed, these coastal eddies can be considered as a link between the coastal water and the open sea and could have an important influence on the coast-offshore transport of nutrients and phytoplankton, as well as heat and energy.

Hence, it is important to understand the physical dynamics of these eddies and, in particular, their generation process. Various dynamical processes can contribute to eddy generation [*McWilliams*, 1985]. For instance, current instabilities are important mechanisms for eddies of the Gulf Stream [e.g. *Robinson and Pinardi*, 1988], or in the Gulf of Mexico [e.g. *Hurlburt and Thompson*, 1980]. The topographical influence is also an important contributor to the Meddies (eddies of Mediterranean Water) formed near Cape Saint Vincent [*Pichevin and Nof*, 1996] and, in general, to all the eddies formed around capes or around headlands [e.g. *Signell and Geyer*, 1991; *Doglioli et al.*, 2004; *Magaldi et al.*, 2010]. The eddies in the lee of the Hawaiian islands are formed as a result of combined wind forcing, topography and instabilities associated with current flow [*Lumpkin*, 1998; *Chavanne et al.*, 2002; *Kersalé et al.*, 2011]. In the Northwestern Mediterranean

basin, *Pascual et al.* [2002] suggested that an eddy observed in the Balearic Sea is created by the wind curl stress. Coastal anticyclonic eddies observed in the eastern part of the GoL [*Allou et al.*, 2010] and in the Catalan Sea [*Rubio et al.*, 2005; *Rubio et al.*, 2009a] are created by a separating branch of the NC due to the topography. *Schaeffer* [2010] also showed that the generation mechanism of anticyclonic eddies in the eastern part of the GoL are related to the local wind conditions. In our study area, *Millot* [1979, 1982] suggested that anticyclonic circulation may arise in the surface layer in the western part of the GoL to compensate the offshore departure of coastal waters following an upwelling phenomena. *Estournel et al.* [2003] and *Petrenko et al.* [2008] also showed that the wind curl over the GoL can create an anticyclonic eddy circulation over the shelf of the gulf by using academic simulations. However, the precise generation mechanism of the eddy located in the western part of the GoL is still not clear. Hence, starting from the hypothesis of *Millot* [1979, 1982], we investigate the generation process of anticyclonic eddies. The present work is carried out within the framework of the LAgrangian Transport EXperiment (LATEX) projet (2008-2011) initiated to study the role of mesoscale eddies on shelf-offshore exchanges in the GoL.

The paper is organized as follows: Section 2 describes the numerical approach as characteristics of modeling, strategy of analysis of wind forcing and eddy identification technique; Section 3 presents the comparison between the numerical results and observations; Section 4 investigates eddy formation process regarding various wind forcing and stratification conditions; the results are discussed in Section 5 and the summary and conclusions are presented in Section 6.

2. Material and method

2.1. Numerical modeling

For the present study, we use Symphonie, a 3-D primitive equation model, with a free surface, hybrid sigma coordinates, based on Boussinesq and hydrostatic approximations [*Marsaleix et al.*, 2006, 2008]. Symphonie has already been used in the area, for example to study the wind-induced circulation in the GoL [*Auclair et al.*, 2003; *Estournel et al.*, 2003; *Petrenko et al.*, 2005, 2008] and dense-water formation and/or cascading phenomena over the continental shelf [*Dufau-Julliand et al.*, 2004; *Ulses et al.*, 2008a, b] and deep convection in the northwestern Mediterranean Sea [*Herrmann and Somot*, 2008; *Herrmann et al.*, 2008]. A C-grid is used for spatial discretization [*Arakawa and Suarez*, 1982]. The second-order closure scheme of *Gaspar et al.* [1990] is used to estimate vertical turbulence. *Hu et al.* [2009] developed and validated an upwind-type advection-diffusion scheme to improve the ability of the model to reproduce coastal mesoscale eddies. In the present application, the model domain extends throughout the whole GoL with a horizontal resolution of 1 km and 40 σ-hybrid vertical levels (Fig. 1). Surface atmospheric forcings are provided by the meteorological model Aladin of Météo-France with high spatial (0.1° x 0.1°) and temporal (3h) resolutions. Initial and open boundary conditions are provided by the Mediterranean Forecasting System (MFS) general circulation model [*Pinardi et al.*, 2003] with a resolution of 1/8°. The original forcing data are bilinearly interpolated in the Symphonie model grid, and linearly interpolated in time. Daily fluxes of fresh water from major rivers (Rhône, Hérault, Aude and Orb), are provided by the *Compagnie Nationale du Rhône*. Based on available data, we have simulated 8 years from January 2001 to December 2008. The daily outputs of current components, salinity, temperature

and density are averaged over 24 hours of simulation for filtering diurnal and/or inertial oscillation (frequency is of 17.5 hours in the GoL corresponding to latitudes around 43° N).

2.2. Wind forcing analysis

In order to study the generation process in response to changes in wind forcings, we use the meteorological wind data used in our numerical simulations. Measured meteorological data are available at terrestrial stations around the GoL, among other at Leucate (Fig. 1). We have compared the Aladin wind with the available measurements and have found a good agreement. In sake of conciseness we do not show this comparison. For this study, to illustrate the wind variability in the western part of the GoL, we have decided to use the Aladin model data at the grid point near the position of the meteorological Leucate station. Indeed, this location represents quite well the changes in the wind forcing in the western part of the GoL, because it is systematically in the path of the NW wind whether it extends spatially or exhibits a strong wind stress curl. In the following we consider that the wind is a 'strong NW wind event' when its amplitude is larger than (or equal to) 8 m.s^{-1} and its direction between 270°and 360°. When the wind amplitude exceeds 14 m.s^{-1}, we define it as an 'extremely strong wind'.

2.3. Eddy identification and tracking

A wavelet signal decomposition is used to analyze the modeled horizontal relative vorticity to identify and follow coherent eddy structures in the numerical simulations [WATERS utility program, *Doglioli et al.*, 2007]. This technique of signal decomposition in orthogonal wavepackets provides both spatial and frequency information and has been largely

used to detect coherent structures in spatial fields. We adjusted the number of spectral components associated with the eddies in order to filter out patterns of incoherent structures such as filaments. To each eddy is associated a group of grid points and a center located at an extremum of the analysed field. Eddy areas may therefore be computed as the sum of gridcell areas. Backward (forward) tracking finds the 'birth' and 'death' of the eddy respectively. Hence we can deduce the life duration of the eddy. More details about the wavelet analysis and WATERS utility program can be found in *Doglioli et al.* [2007]. More recently, WATERS has been used by *Dencausse et al.* [2010] to study the routes of Agulhas rings and by *Rubio et al.* [2009b] to investigate mesoscale activity in the Benguela upwelling system. In the present work, analysis is performed at 20-m depth because, during the stratified season, it is about half the mixed layer depth over which the eddies extend. We performed the wavelet analysis to the 8 years of simulated horizontal relative vorticity field in order to identify all anticyclonic eddies present in the western part of the GoL and to track their life duration. The backward tracking in time of an identified eddy till its 'birth' helps us investigate its formation.

3. Validation of the Modeling

The capability of the Symphonie model of reproducing the mesoscale circulation over the shelf in the GoL has been demonstrated by previous studies [*Estournel et al.*, 2003; *Petrenko et al.*, 2005, 2008; *Dufau-Julliand et al.*, 2004; *Ulses et al.*, 2008a]. Here we present a short comparison between the ADCP, drifters and XBT data gathered during the experiment Latex08 and the simulation carried out on the year 2008. The Latex08 cruise took place from September 1 to 5, 2008 on board the RV *Téthys II* and more details of the experiment is given in *Hu et al.* [2011].

The ADCP data measured at 15 m depth along transect A (B) on Sept. 1 (Sept. 5) and the trajectories of the drifters from Sept. 5 to 11 are shown in Fig. 2-a. The northward (western part) and the southward (eastern part) currents along the transect A, the eastward (northern part) and westward (southern part) currents along the transect B reveal a continuous rotational clockwise circulation associated with an anticyclonic eddy. The drifters' trajectories, following the outer edge of the eddy, illustrate its elliptic shape. The corresponding simulated currents along the same ship's tracks are shown in Fig. 2-b. The observed anticyclonic eddy is reproduced by the model results as identified by the dark gray contour issued from wavelet analysis on Sept. 10 and by the modeled clockwise circulation along the transect A. The major pattern of the eddy agree with the observations, although the intensity and the horizontal dimension of the simulated eddy is slightly less than that of the observed one. The simulated eddy is more northwest and on-shore in position than the observed one. The observed clockwise rotation along the transect B is not reproduced since the transect B, crossing most diagonally the observed eddy, is on the outer edge of the simulated one. In the south extremity of the transect B, the modeled southwestward current with the same intensity as the eddy suggests the presence of the NC, which is not described by the observations. Since the sea state during the cruise did not allow the use of the CTD we had on board, no deep comparison of hydrological fields could be applied with the simulation. Nevertheless, we have just one temperature profile measured by an XBT (marked as black cross in Fig. 2-a) and we propose a comparison with the model results in Fig. 3. At the surface, the discrepancy between the observed and modeled temperature is less than $0.2°C$. Vertically, the observed thermocline is about 35 m depth, while the modeled one is about 5-10 m deeper. Although the measured XBT

profile is stopped at 200 m depth, the temperature at depth below can be considered to be about $13.4°C$, which becomes stable from 60 m depth and presents the typical temperature of the Modified Atlantic Water (MAW) in this area [*Albérola and Millot*, 2003]. Below the thermocline till 250 m depth, the important gradient between the modeled temperature and the observed one is related to the presence of the NC [*Petrenko et al.*, 2005] at the XBT position in the model results as shown by ADCP data in Fig. 2-b. From 250 m depth to the bottom, the modeled temperature is again in a good agreement with the observed one.

One should note that the 24 hours averaged daily model outputs are not expected to reproduce the high variability of the circulation due to the wind. The goal of the present simulation is not to reproduce exactly the observed anticyclonic eddy but to reproduce the most the mesoscale dynamic process in order to help us understand the eddies' generation mechanism. Previous simulation by *Hu et al.* [2009] with the same model configuration as the present one was carried out on year 2001, present a good reproduction of realistic anticyclonic eddies in the GoL. The present simulation is run with the same configuration over 8 years, prolongating from 2001 till 2008. Combined satellite observations over 8 years of simulation (not shown) and field observation on 2008 show that the model is able to reproduce the mesoscale eddies in the western part of the GoL and their major patterns over the whole simulated period and can hence to serve as a tool to investigate eddy's generation process.

4. Results

We examined the 8 years of simulated horizontal relative vorticity field and found that, in the western part of the GoL, anticyclonic features can be observed all year around.

194 However, the anticyclonic features formed during winter and spring time are weak in in-
195 tensity and smaller in size than the internal Rossby radius which is suggested to be 15 km
196 in this region [*Grilli and Pinardi*, 1998]. Generally lasting only 2-3 days, they do not
197 consist of closed loops and hence are not considered as coherent eddy structures. In con-
198 trast, coherent, strong and more lasting anticyclonic eddy structures occur between May
199 and October. These anticyclonic eddies generally consist of warm, less salty buoyant wa-
200 ter with a positive sea-surface height anomaly (SSHA) comparing to the ambient waters.
201 The features of these modeled eddies are in agreement with previous observations [*Millot*,
202 1979; *Hu et al.*, 2011]. The application of the wavelet analysis on all simulated coherent
203 eddies in the simulations shows that these mesoscale anticyclonic eddies are about 20 km
204 in diameter during their developing phase. Their horizontal dimension increases with time
205 to be 80 km when they get fully developed. Tracking analysis of these eddies shows that
206 their life durations vary from several days to a couple of months.

207 In the present work, we define as 'long-life' eddies the anticyclonic eddies which last at
208 least 15 days, in opposition to the other ones that we call 'short-life' eddies. The 'long-
209 life' is defined relatively to 'short-life' for the eddy structures in such a coastal study area,
210 and hence can not be compared to the lifetimes of the open ocean eddies as for example
211 the Agulhas Rings or the Algerian basin anticyclones. Regarding the actual conventions
212 to separate submeso- and meso-scale, our short-life eddies belong probably to the first
213 category and the long-life ones to the second one. In the 8 years of simulations, 8 long-life
214 anticyclonic eddies have been observed (Table 1). These long-life eddies occur during a
215 three-month period, between July and early October. No long-life eddy was detected in
216 2004 and in 2007. The first or the unique eddy generally appears in July (in the following

indicated with A1 followed by the year, e.g. A1_2001), as it occurs 5 years out of the 6 during which eddies are present (2001, 2002, 2003, 2005 and 2008). The life durations of these first eddies range from 38 to 76 days, except for the 2006 eddy, which starts at the beginning of August and disappears at the end of that month lasting only 28 days. In 2003 and 2005, two long-life eddies have been detected successively during the three-month period. Both second eddies (indicated as A2 followed by the year) begin around mid-September and disappear early October lasting 15 and 26 days. Hence they generally last a shorter time than their July counterparts. Over the 8 years of simulations, we observe long-life eddies 5 times in July, 6 times in August, 5 times in September and 3 times in early October. In summary, the period when a long-life anticyclonic eddy is more likely to be encountered in the western part of the GoL extends from July to early October with the highest probability in August.

We present in Fig. 4 an example of an anticyclonic eddy formed in the western part of the GoL each year. These coastal eddies are rarely round in shape and have generally an elliptic form with a zonal major axes along the western coast (Fig. 4). The horizontal dimension of the modeled eddy seems to be limited by the curvature of the western coastline. The irregular contour edge like the small 'tail' in the south edge of the eddy A1_2001 (Fig. 4-a) suggests the interaction of the eddy with the NC or surrounding currents. Eddy A1_2002 (Fig. 4-b) is smaller than the other eddies and is quite close to the coast. Eddy A2_2003 (Fig. 4-d) and eddy A2_2005 (Fig. 4-f) are located more off-shore than the others. These eddies are all generated in the same area near the Roussillon coast at around 43°N, 3°15'E. The diameter [1] of the eddies ranges from 10-20 km when they are newborn to 50-80 km when they are well-developed. After their generation, the

eddies have slight meridional or off-shore displacement to end up where they are shown on Fig. 4. The NC located at their south-southeast edge (Fig. 1), combined with the presence of Cape Creus, plays the role of a barrier, and constrains the eddies within the western part of the GoL.

No long-life eddies have been detected in 2004 and 2007. However, the circulations over the shelf during these two years are quite different. In 2004, only short-life anticyclonic features occur. In 2007, a large northeastward countercurrent (sensu [*Petrenko et al.*, 2008]), but not a closed anticyclonic eddy, occupies the whole west part of the GoL from late May till late October (Fig. 4-h). The south-east edge of this circulation consists of the NC along the continental slope.

4.1. Influence of wind forcing

It was demonstrated in previous studies [*Millot*, 1979, 1982; *Estournel et al.*, 2003; *Petrenko et al.*, 2008] that the coastal eddies/circulations in the GoL are strongly dependent on the wind event in this region. In the first phase, we attempt to investigate the influence of wind forcing on eddy generation. Since the NW wind is quite frequent in this area over the whole year, in order to investigate the eddy generation in response to wind forcing, we have tried to find a situation where a strong burst of northwest wind occurs after a quiet period to take it as a 'reference' situation. This allows us to avoid the potential remnant effect of a previous wind event on the circulation. Hence, we have chosen to first concentrate on 2005 and show the simple case of the A1_2005 eddy (Fig. 5). Following a quiet period with no wind, the wind starts blowing on June 30, 2005. It lasts until July 13 (with one day of recession on July 4). It creates the long-life eddy A1_2005 observed from

July 10 till September 4, hence lasting 57 days. The figures selected in Fig. 5 illustrate different stages during the eddy's formation.

As mentioned earlier, from June 26 to 28, there is no strong wind in the western part of the GoL (Fig. 5-a). On June 28, the currents along the Roussillon coast are southward over the entire water column with a decrease in magnitude with depth (Fig. 5-e,i). A strong NW wind blows almost persistently from June 30 to July 2 through the whole shelf with a maximum wind intensity of 15 ms^{-1} (Fig. 5-b). Offshore, the surface water over the shelf near the north and north-east coast around the Cape d'Agde is advected south-southwestward in response to Ekman transport perpendicular to the wind direction (Fig. 5-f). The sea surface level close to the north coast is depressed in consequence. An on-shore current is observed at deeper depth partially compensating for the upwelled waters (Fig. 5-j). The surface southwestward Ekman transport is reinforced and constrained by the inner edge of the NC surface layer. Reciprocally, the NC itself is accelerated by the wind-derived circulation and becomes an even stronger barrier preventing the outlet of the southwestward Ekman transport into the Catalan sea. The water piles close to Cape Creus and creates a high SSHA around the cape. The NW wind is absent on July 4 (not shown) but rises again the day after. The same process repeats itself and the SSHA near the west coast increases. On July 6, the north-south surface pressure gradient starts to create a northward current along the Roussillon coast (Fig. 5-k). This northward coastal current follows the curved shape of the Roussillon coast. It then turns to the open sea near the Cape d'Agde and joins the southwestward off-shore current. This creates an anticyclonic structure while the surface current is still governed by the wind and keeps its southwestward on-shore movement and keeps on accumulating near the coast. On July

10, the wavelet analysis detects the 'birth' of the eddy. The shape of this eddy identified by the wavelet analysis at 20 m depth corresponds well with the relative high SSHA at the surface associated with the eddy structure. The eddy is about 20-30 km in diameter and extends through the mixed layer. The advected warm water from the shelf surface accumulated near the western coast is the water source for this anticyclonic eddy. The strong NW wind persists for 9 days until July 13. The eddy, fed continually under the same process by the coastal northward jet current, increases in size and intensity. At the end of this persisting NW wind event, the eddy has an approximate north-south elliptical shape and is about 30-40 km in diameter (Fig. 6-d). The 'tail' at its southern edge reveals its interaction with the NC. The eddy location is more south than its initial location. The eddy weakens when the supply process of wind-driven energy stops. From July 14 to 18, the NW wind disappears for 5 days. By the end of this no wind period, the eddy size has reduced to almost half. The eddy has slightly moved southward to the coast (Fig. 6-e) following the relaxation of the surface pressure gradient. The eddy intensity has also decreased and its shape has become more elongated. Afterwards, several strong NW wind events occur in succession with little gaps between them until August 20. At this time, the eddy has become a quite intense structure, less elongated and is about 50 km in diameter (Fig. 6-f).

The same work has been performed on all the simulated anticyclonic structures in the western part of the GoL for the 8 years of simulations. It shows that the wind-driven generation mechanism of the eddy A1_2005 is valid for all other eddies, long-life eddies as well as short-life ones. A systematic analysis is done calculating the percentage of strong NW wind events, with two thresholds (one $\geq$ 8 ms^{-1} and the other one $\geq$ 14

ms^{-1}), during the last three days at Leucate station from May 1 to October 31 for the 8 years of simulations (Fig. 7). The presences of long-life anticyclonic eddies (black thick lines) and short-life anticyclonic features (gray thick lines) within this period reveal very clearly the correlation between the persistent NW wind event and the eddies' generation. In general, a strong NW wind event persisting more than about 75% during 3 days is a necessary condition to have an anticyclonic structure formed in the study zone. A sensitivity analysis has been done on the percentage of the NW wind, varying the period from 1 to 5 days. The results show that the period of 3 days has the best correlation with the eddy's formation. If the percentage does not reach 75%, but the wind persists for more than 3 days, the cumulative effects of the wind can also generate eddies like the two short-life eddies of early July 2001 (Fig. 7-a) and early May 2003 and like the long-life eddy A1_2003 (Fig. 7-c). Moreover, a strong NW wind is also necessary after the eddy's formation to sustain the structure. For instance, in 2006, only one persistent NW wind event occurs around July 7 and creates an eddy structure (Fig. 7-f). No more persistent NW wind occurs after its formation; hence the eddy disappears after existing only 5 days and hence is not classified as a 'long-life' eddy. While in early August, the NW wind, persisting for more than half a month, creates the long-life eddy A1_2006.

4.2. Influence of stratification conditions

Strong NW wind events may arise at any time of the year in this area. However, coherent eddies occur only between May and October, while during winter-spring season, no eddies can be formed even if a strong NW wind event is satisfied. The high probability of observing a long-life anticyclonic eddy during the summer season suggests that the stratification condition probably plays a role on the eddy's generation dynamics. Hence, in the

second phase, the influence of stratification condition on eddy generation is investigated. In order to study the annual variation of the stratification, the potential energy anomaly ϕ is chosen as the indication of the stability of the water column. This parameter is defined by *Simpson* [1981] and *Simpson and Bowers* [1981] as:

$$\phi = \frac{1}{D}\int_{-H}^{\eta} gz(\bar{\rho} - \rho)dz \tag{1}$$

with the depth-mean density $\bar{\rho}$ defined as:

$$\bar{\rho} = \frac{1}{D}\int_{-H}^{\eta} \rho dz \tag{2}$$

where ρ is the density, H the bathymetry, η the sea surface elevation, $D = H + \eta$ the water column depth and g the gravitational acceleration. For a given density profile, ϕ represents the amount of mechanical energy required to instantaneously homogenize the water column. This parameter has been used successfully as a criterion to study the phenomena concerning stratification [*Burchard and Burchard*, 2008; *De Boer et al.*, 2008; *Schaeffer*, 2010]. The value of ϕ decreases with the level of homogeneity through the water column. Higher values of ϕ indicate a stronger stratification.

During the winter-spring season, ϕ is minimum in magnitude with a value less than 20 Jm^{-3}, indicating a weak stratification (Fig. 8). In general, the increase of ϕ in early May indicates the establishment of the seasonal stratification variation. ϕ reaches a maximum value late June, stays at this level about 3 months till late September and then diminishes with the fall/winter mixing. July, August and September are the months with the maximum value ϕ of about 100 Jm^{-3}. The most stratified conditions are observed during these months and coincidence with the occurrence of all the long-life eddies. We note that ϕ is relatively smaller in 2002 and 2004 with a value of about 60 Jm^{-3} during July-September

compared with the value of ϕ of all the other years. Hence, three stratified conditions can be defined by the range of the ϕ value: 1) a weak stratification with a value ϕ below 20 Jm^{-3}, as the one in winter-spring season; 2) an intermediate stratification with a value ϕ around 60 Jm^{-3}; as the one in early May and late October of all years and during the summer season in 2002 and 2004; 3) a strong stratification with a value ϕ reaching 100 Jm^{-3}, as during all summer seasons except 2002 and 2004. In 2004, no long-life eddy ever occurs despite the successive NW wind events. We think that this is due to the too weak stratification of that summer. The year 2005 is used again to demonstrate the influence of stratification. A short-life eddy, referred as A0_2005, is present in early May. Eddy A0_2005 is born on May 8 and disappears on May 18, lasting only 11 days. The strength and horizontal size of this short-life eddy are almost one third the ones of long-life eddy A1_2005 (Fig. 9-Left) that lasts 57 days from July 10 till September 4. The vertical extent of both anticyclonic eddies, clearly revealed by the areas with high magnitude of current intensity associated with the eddy rotation, is about 30-35 m depth (40-50 m) for the eddy A0_2005 (A1_2005) (Fig. 9-Middle). Vertical transects of density show that both eddies are vertically constrained by the thermocline and hence have baroclinic characteristics (Fig. 9-Right). The deepening of the pycnocline in both vertical sections is due to the eddy-induced downwelling within an anticyclonic structure. Excluding the eddy deepening effect, the mixing layer depth ($\sim$ 20m) in early May is shallower than the one in mid-August ($\sim$ 40m). The density gradient between the surface mixed layer and the deeper layer is also less in May than in August. Both differences indicate that the stratification in early May is weaker than in August, in accordance with the evolution of ϕ.

The long-life eddy A1_2005 is hence deeper in vertical extent and has more buoyant water within its core compared to the short-life eddy A0_2005.

The differences of eddy characteristics between A0_2005 and A1_2005 can be observed between the other short-life and long-life eddies. Such differences, combined with the evolution of the density stratification, suggest that the eddy's size, vertical extent, strength and life duration increase with the stratification condition. During winter-spring, the vertical water column is almost homogenous, and hence is not favorable to eddy generation. The July to September period exhibits the most stratified condition, and hence all the long-life eddies occur within this period. May, June and October have a stratification stronger than the winter-spring one, but smaller than the July-September one. The structures occurring during these 3 months are therefore intermediate in nature, more stable than the filaments observed in winter-spring, but smaller, shallower and less intense than the long-life eddies of July-September. Hence, to have a long-life anticyclonic eddy in the western part of the GoL, the second necessary condition, in addition to strong NW wind events, is a strong stratification.

5. Discussion

To have a long-life anticyclonic eddy in the western part of the GoL, both persistent strong NW wind events and a well-stratified water column are necessary conditions. As described by *Crépon and Richez* [1982] in their analytical study of coastal upwelling, symmetric offshore wind jets blowing perpendicular to the coast can generate offshore upwellings with extension of the order of the internal radius of deformation; anticyclonic (cyclonic) eddies may arise to the right (left) side of the wind axis (looking downwind) due to the spatial variation of wind stress and downward (upward) Ekman pumping associated.

Based on their analytical solutions, *Hua and Thomasset* [1983] numerically studied the wind-induced upwelling in the GoL, and revealed that upwelling center can be located near the segment of the coastline from Leucate to cape d'Agde. Anticyclonic eddies formed following an upwelling in this area are present on the right side of the Tramontane jet and have a size of the order of the Rossby radius of this area when they begin to be formed. Their size increases with time to about 80 km when they get fully developed. No cyclonic counterpart has been observed in the eastern part of the GoL like the symmetric vortex illustrated by *Crépon and Richez* [1982], this might be explained by the variability of the coastline. The component of the NW Tramontane wind perpendicular to the north-east coast is very small due to the curvature of the coastline [*Hua and Thomasset*, 1983]. Similar situations have been described in the gulf of Tehuantepec in the eastern tropical Pacific Ocean, where mesoscale anticyclonic eddies are induced by strong, offshore winds [*Trasvinã et al.*, 1995; *Willett et al.*, 2006] in the western gulf. They are also present in the right side (since it is in the Northern hemisphere) of the axis of the wind and are several times the Rossby radius. Flow pattern in the gulf of Tehuantepec also shows an asymmetric feature with no corresponding cyclone presenting in the eastern gulf. *Trasvinã et al.* [1995] showed that, in their case, the entrainment associated with wind stirring is responsible for the weakening of the cyclonic eddies and that the uplifted thermocline which maintains the cyclonic eddy is weakened by the mixing process. The analytical study by *Crépon and Richez* [1982] also showed that the upwelling is linked to the motion of the interface generated by baroclinic mode and is dependent on the stratification. This also explains the importance of the stratification condition on the generation of eddies following the upwelling phenomenon in this area. If we consider the energy cycle as

presented by *Böning and Budich* [1992], the injection of energy by the NW wind can be transferred into potential energy (PE) when the wind-driven Ekman transport pushes the buoyant surface water to the west coast near Cape Creus and downward locally. The eddy generation is driven primarily through the release of PE by baroclinic process [*Holland and Haidvogel*, 1980; *Ferrari and Wunsch*, 2009]. The mean field PE can also be converted into eddy PE by baroclinic process [*Böning and Budich*, 1992]. In another words, in our case, strong wind events are the source of energy, and a well-stratified condition favors the transfer of this wind-induced energy to eddy kinetic energy.

The percentage of the NW wind presence and its maximum and average amplitude from May 1 till October 31 is computed for the 8 years of simulations in order to quantitatively estimate the wind forcing (Table 2). The combined effect of both factors but with different levels, resulting in differences of eddy's formation, is discussed in the following six cases: i) when no persistent NW wind event is present, whether stratification is strong or not, no eddy formation occurs. ii) Instead, when a persistent NW wind event occurs while stratification is weak, anticyclonic filaments are generated like the ones formed during winter-spring. iii) When a persistent NW wind event occurs with an intermediate stratification, eddy structures can arise but they possess a short life duration, small size, shallow depth and weak intensity. They correspond to the short-life eddies formed in May, June and late October. In 2004, stratification during July-September is not as strong as during the other years (Table 2). Only several persistent NW wind events occur in July, creating transients eddies, but are absent from August to late September (Fig. 7-d) and

no long-life structures have been detected in 2004. iv) When extremely strong persistent NW wind events occur, long-life eddies can exist despite the intermediate stratification. The long-life eddy A1_2002 is generated in this situation. Indeed, the stratification during summer 2002 is similar to the one in 2004 (Fig. 8), implying that summer 2002 is not favorable to long-life eddies. Nonetheless, in 2002, the NW wind has the maximum average intensity (20 ms^{-1}) over the 8 years (Table 2). Moreover its percentage of 59% is the second highest one after 2007. In fact the strong wind bursts are also especially concentrated from July to August (Fig. 7-b). Despite the stratification but thanks to the strong energy injection, the long-life anticyclonic eddy A1_2002 is formed but with a size smaller than the ones of the other long-life ones (Fig. 4). v) When persistent NW wind events and a strong stratification coexist, intense, long-life eddy can be generated. The other 7 long-life eddies: A1_2001, A1_2002, A1_2003, A2_2003, A1_2005, A2_2005 and A1_2008 are generated in this case. In 2006, the long-life eddy lasts only 22 days. 2006 is the year with the least presence of long-life eddy (Table 1). This can be explained by the fact that 2006 has the minimum percentage of the NW wind (47%) of all during this 8-year period. Moreover, the wind has a weak intensity, comparable with the one in 2004. However, the strong stratification in 2006 compensates for the weak wind forcing hence the long-life eddy A1_2006 exists but with a shorter duration. vi) When extremely strong persistent NW wind events occur with a strong stratification, the anticyclonic eddy increases in scale and becomes an anticyclonic circulation like the one observed in 2007 (Fig. 4-h). Indeed, on one hand, the stratified condition in 2007 present from late June till late October, is quite strong as shown in Fig. 8. On the other hand, the NW wind in 2007 has the largest percentage (62%) of all years and its intensity is the seconder highest. Both conditions

for eddy formation are more than satisfied; hence such anticyclonic circulation can be considered as an extreme case of an eddy-like structure.

6. Summary and conclusion

A realistic numerical model has been used in the present work to study the generation of mesoscale anticyclonic eddies located in the western part of the GoL between January 2001 and December 2008. Eddy's life duration varies from several days to several months. During the 8 years of simulation, 8 long-life anticyclonic eddies with a life duration longer than 15 days have been detected. They all occur between July and early October. Compared with the short-life structures occurring in May, June and late October, the long-life eddies have a bigger size, a deeper vertical extension and are more intense. Indeed, the simulated long-life eddies have dimensions of the same order of the Rossby radius of this area at the beginning of their life. Their size increases with time and becomes several times the Rossby radius when they get fully developed. The simulated eddies are baroclinic, as the *in situ* anticyclonic eddy observed in early September 2008 in the study area during the Latex08 cruise [*Hu et al.*, 2011].

The formation process can be described schematically by Fig. 10. A strong NW wind persisting at least 75% of the previous 3 days induces an Ekman transport piling the water close to Cape Creus (Fig. 10-a). A northward current along the Roussillon coast is created (Fig. 10-b). This current turns to its right approaching Cape d'Agde and generates an anticyclonic circulation (Fig. 10-c) that is the precursor of an anticyclonic eddy. After this initial generation phase, the results show that persistent NW wind and a strong stratification guarantee the generation of a long-life eddy in the western part of the GoL. Different cases can be found varying the combination of these two conditions,

hence leading to situations from short-life eddies to extended anticyclonic circulation. Hence, this work explains in details the generation mechanism of the eddy, first observed by *Millot* [1979, 1982]. Moreover, it could be used to improve the short-term numerical predictability of the complex coastal circulation in the study area.

Acknowledgments. The LATEX projet is supported by the programs LEFE/IDAO and LEFE/CYBER of the INSU-Institut National des Sciences de l'Univers and by the Region PACA-Provence Alpes Côte d'Azur. The meteorological data were kindly supplied by Météo-France. We acknowledge the MFSTEP program for OGCM outputs. Z.Y. Hu is financed by a MENRT Ph.D. grant.

Notes

1. Elliptical diameter defined as the mean of the minor and major axes.

References

Albérola, C., and C. Millot (2003), Circulation in the French Mediterranean coastal zone near Marseilles: the influence of the wind and the Northern Current, *Cont. Shelf Res.*, *23*, 587–610.

Albérola, C., C. Millot, and J. Font (1995), On the seasonal and mesoscale variabilities of the Northern Current during the PRIMO-0 experiment in the western Mediterranean Sea, *Oceanol. Acta*, *18*, 163–192.

Allou, A., P. Forget, and J. Devenon (2010), Submesoscale vortex structures at the entrance of the Gulf of Lions in the Northwestern Mediterranean Sea, *Cont. Shelf Res.*,

30(7), 724 – 732, doi:DOI:10.1016/j.csr.2010.01.006.

Arakawa, A., and M. Suarez (1982), Vertical Differencing of the Primitive Equations in Sigma Coordinates, *Mon. Wea. Rev.*, *111*, 34–45, doi:10.1175/1520-0493(1983)111.

Auclair, F., P. Marsaleix, and P. De Mey (2003), Space-time structure and dynamics of the forecast error in a coastal circulation model of the Gulf of Lions, *Dyn. Atmos. Oceans*, *36*, 309–346, doi:10.1016/S0377-0265(02)00068-4.

Böning, C. W., and R. G. Budich (1992), Eddy dynamics in a primitive equation model : sensitivity to horizontal resolution and friction, *J. Phys. Oceanogr.*, *22*, 361–381.

Burchard, H., and R. Burchard (2008), A dynamic equation for the potential energy anomaly for analysing mixing and stratification in estuaries and coastal seas, *Estuarine, Coastal Shelf Science.*, *77*(4), 679 – 687, doi:DOI:10.1016/j.ecss.2007.10.025.

Chavanne, C., P. Flament, R. Lumpkin, B. Dousset, and A. Bentamy (2002), Scatterometer observations of wind variations induced by oceanic islands: implications for wind-driven ocean circulation., *Canadian Journal of Remote Sensing*, *28*(3), 466–474.

Crépon, M., and C. Richez (1982), Transient upwelling generated by 2-d atmospheric forcing and variability in the coastline., *J. Phys. Oceanogr.*, *12*, 1437–1457.

De Boer, G. J., J. D. Pietrzak, and J. C. Winterwerp (2008), Using the potential energy anomaly equation to investigate tidal straining and advection of stratification in a region of freshwater influence, *Ocean Model.*, *22*, 1–11.

Dencausse, G. J., M. Arhan, and S. Speich (2010), Routes of Agulhas rings in the south-eastern Cape Basin, *Deep-Sea Res. I*, *57*, 1406–1421, doi:10.1016/j.dsr.2010.07.008.

Doglioli, A., A. Griffa, and M. Magaldi (2004), Numerical study of a coastal current on a steep slope in presence of a cape: The case of the Promontorio di Portofino,

J. Geophys. Res., *109*, C12033, doi:10.1029/2004JC002422.

Doglioli, A. M., B. Blanke, S. Speich, and G. Lapeyre (2007), Tracking coherent structures in a regional ocean model with wavelet analysis: application to Cape Basin Eddies, *J. Geophys. Res.*, *112*, C05043, doi:10.1029/2006JC003952.

Dufau-Julliand, C., P. Marsaleix, A. Petrenko, and I. Dekeyser (2004), Three-dimensional modeling of the Gulf of Lion's hydrodynamics (northwest Mediterranean) during January 1999 (MOOGLI3 Experiment) and late winter 1999: Western Mediterranean Intermediate Water's (WIW's) formation and its cascading over the shelf break, *J. Geophys. Res.*, *109*, C11002, doi:10.1029/2003JC002019.

Echevin, V., M. Crepon, and L. Mortier (2003), Interaction of a coastal current with a gulf: application to the shelf circulation of the Gulf of Lions in the Mediterranean Sea, *J. Phys. Oceanogr.*, *33*, 188–206.

Estournel, C., V. Kondrachoff, P. Marsaleix, and R. Vehil (1997), The plume of the Rhône: numerical simulation and remote sensing, *Cont. Shelf Res.*, *17*(8), 899–924, doi:DOI:10.1016/S0278-4343(96)00064-7.

Estournel, C., X. Durrieu de Madron, P. Marsaleix, F. Auclair, C. Julliand, and R. Vehil (2003), Observation and modeling of the winter coastal oceanic circulation in the Gulf of Lions under wind conditions influenced by the continental orography (FETCH experiment), *J. Geophys. Res.*, *108*(C3), 7–18, doi:10.1029/2001JC000825.

Ferrari, R., and C. Wunsch (2009), Ocean Circulation Kinetic Energy: Reservoirs, Sources, and Sinks, *Annu. Rev. Fluid Mech.*, *41*, 253–282, doi:10.1146/annurev.fluid.40.111406.102139.

Flexas, M. M., X. Durrieu de Madron, M. A. Garcia, M. Canals, and P. Arnau (2002), Flow variability in the Gulf of Lions during the MATER HFF experiment (March-May 1997), *J. Mar. Sys.*, *33-34*, 197 – 214, doi:DOI:10.1016/S0924-7963(02)00059-3.

Gaspar, P., Y. Grégoris, and J.-M. Lefevre (1990), A simple eddy kinetic energy model for simulations of the oceanic vertical mixing: Tests at Station Papa and long-term upper ocean study site, *J. Geophys. Res.*, *95*, 179–193.

Grilli, F., and N. Pinardi (1998), The computation of Rossby radii dynamical processes of deformation for the Mediterranean Sea, *MTP News*, *6*, 4.

Herrmann, M., S. Somot, F. Sevault, C. Estournel, and M. Déqué (2008), Modeling the deep convection in the northwestern Mediterranean Sea using an eddy-permitting and an eddy-resolving model: Case study of winter 1986-1987, *J. Geophys. Res.*, *113*, C04011, doi:10.1029/2006JC003991.

Herrmann, M. J., and S. Somot (2008), Relevance of ERA40 dynamical downscaling for modeling deep convection in the Mediterranean Sea, *Geophys. Res. Lett.*, *35*, L04607, doi:10.1029/2007GL032442.

Holland, W. R., and D. B. Haidvogel (1980), A parameter study of the mixed instability of idealized ocean currents, *Dyn. Atmos. Oceans*, *4*(3), 185 – 215, doi:DOI:10.1016/0377-0265(80)90014-7.

Hu, Z. Y., A. A. Doglioli, A. M. Petrenko, P. Marsaleix, and I. Dekeyser (2009), Numerical simulations of eddies in the Gulf of Lion, *Ocean Model.*, *28*(4), 203 – 208, doi:DOI:10.1016/j.ocemod.2009.02.004.

Hu, Z. Y., A. A. Petrenko, A. M. Doglioli, and I. Dekeyser (2011), Study of coastal eddies: application in the Gulf of Lion, *J. Mar. Sys.*, *88*, 3–11, doi:10.1016/j.jmarsys.2011.02.

008.

Hua, B., and F. Thomasset (1983), A Numerical Study of the Effects of Coastline Geometry on Wind-Induced Upwelling in the Gulf of Lions, *J. Phys. Oceanogr.*, *13*, 678–694.

Hurlburt, H. E., and J. D. Thompson (1980), A numerical study of Loop Current intrusions and eddy shedding in Gulf of Mexico, *J. Phys. Oceanogr.*, *10*, 1611–1631.

Huthnance, J. M. (1995), Circulation, exchange and water masses at the ocean margin: the role of physical processes at the shelf edge, *Prog. Oceanogr.*, *35*(4), 353 – 431, doi:DOI:10.1016/0079-6611(95)80003-C.

Kersalé, M., A. M. Doglioli, and A. A. Petrenko (2011), Sensitivity study of the generation of mesoscale eddies in a numerical model of hawaii islands, *Ocean Sci.*, *accepted*.

Ludwig, W., E. Dumont, M. Meybeck, and S. Heussner (2009), River discharges of water and nutrients to the Mediterranean and Black Sea: Major drivers for ecosystem changes during past and future decades?, *Prog. Oceanogr.*, *80*(3-4), 199–217, doi: 10.1016/j.pocean.2009.02.001.

Lumpkin, C. F. (1998), Eddies and currents in the Hawaii islands, Ph.D. thesis, University of Hawaii.

Magaldi, M., T. Özgökmen, A. Griffa, and M. Rixen (2010), On the response of a turbulent coastal buoyant current to wind events: the case of the Western Adriatic Current, *Ocean Dynam.*, *60*, 93–122, 10.1007/s10236-009-0247-9.

Marsaleix, P., F. Auclair, and C. Estournel (2006), Considerations on Open Boundary Conditions for Regional and Coastal Ocean Models, *J. Atmos. Ocean. Technol.*, *23*, 1604–1613, doi:10.1175/JTECH1930.1.

590 Marsaleix, P., F. Auclair, J. Floor, M. Herrmann, C. Estournel, I. Pairaud, and C. Ulses
591 (2008), Energy conservation issues in sigma-coordinate free-surface ocean models,
592 *Ocean Model.*, *20*, 61–89, doi:10.1016/j.ocemod.2007.07.005.

593 McWilliams, J. C. (1985), Submesoscale, coherent vortices in the ocean, *Rev. Geophys*,
594 *23*(2), 165–182, doi:10.1029/RG023i002p00165.

595 Millot, C. (1979), Wind induced upwellings in the Gulf of Lions, *Oceanol. Acta*, *2*, 261–
596 274.

597 Millot, C. (1982), Analysis of upwelling in the Gulf of Lions, *Hydrodynamics of semi-*
598 *enclosed seas: Proceedings of the 13th International Liège Colloquium on Ocean Hydro-*
599 *dynamics. Elsevier Oceanogr. Ser.*, *34*, 143–153.

600 Millot, C. (1990), The Gulf of Lions' hydrodynamics, *Cont. Shelf Res.*, *10*, 885–894, doi:
601 10.1016/0278-4343(90)90065-T.

602 Millot, C. (1991), Mesoscale and seasonal variabilities of the circulation in the west-
603 ern Mediterranean, *Dynamics of Atmospheres and Oceans*, *15*, 179–214, doi:10.1016/
604 0377-0265(91)90020-G.

605 Millot, C. (1999), Circulation in the Western Mediterranean Sea, *J. Mar. Sys.*, *20*, 423–
606 442, doi:10.1016/S0924-7963(98)00078-5.

607 Millot, C. (2003), Circulation in the Mediterranean Sea and consequences on the water
608 quality, *EGS - AGU - EUG Joint Assembly, Abstracts from the meeting held in Nice,*
609 *France, 6 - 11 April 2003.*

610 Minas, M., and H. Minas (1989), Primary production in the Gulf of Lions with consider-
611 ations to the Rhône River input, *Water Pollution Research Reports*, *32*(5), 112–125.

612 Pascual, A., B. Buongiorno Nardelli, G. Larnicol, M. Emelianov, and D. Gomis (2002), A
613 Case of An Intense Anticyclonic Eddy In The Balearic Sea (w Mediterranean), *J. Geo-*
614 *phys. Res.*, *107*, 3183, doi:10.1029/2001JC000913.
615 Petrenko, A. A. (2003), Variability of circulation features in the Gulf of Lion NW Mediter-
616 ranean Sea. Importance of inertial currents, *Oceanol. Acta*, *26*, 323–338.
617 Petrenko, A. A., Y. Leredde, and P. Marsaleix (2005), Circulation in a stratified and
618 wind-forced Gulf of Lions, NW Mediterranean Sea: *in situ* and modeling data,
619 *Cont. Shelf Res.*, *25*, 7–27, doi:10.1016/j.csr.2004.09.004.
620 Petrenko, A. A., C. Dufau, and C. Estournel (2008), Barotropic eastward currents in
621 the western Gulf of Lion, northwestern Mediterranean Sea, during stratified conditions,
622 *J. Mar. Sys.*, *74*(1-2), 406–428, doi:DOI:10.1016/j.jmarsys.2008.03.004.
623 Pichevin, T., and D. Nof (1996), The eddy cannon, *Deep-Sea Res. I*, *43*(9), 1475 – 1507,
624 doi:DOI:10.1016/S0967-0637(96)00064-7.
625 Pinardi, N., et al. (2003), The Mediterranean ocean forecasting system: first phase of
626 implementation (1998-2001), *Ann. Geophys.*, *21*, 3–20.
627 Robinson, M. A. S., A. R., and N. Pinardi (1988), Gulf Stream simulations and the
628 dynamics of ring and meander processes, *J. Phys. Oceanogr.*, *18*, 1811–1853.
629 Rubio, A., P. Arnau, M. Espino, M. Flexas, G. Jordà, J. Salat, J. Puigdefàbregas, and
630 A. S.-Arcilla (2005), A field study of the behaviour of an anticyclonic eddy on the
631 Catalan continental shelf (NW Mediterranean), *Prog. Oceanogr.*, *66*(2-4), 142–156, doi:
632 10.1016/j.pocean.2004.07.012.
633 Rubio, A., B. Barnier, G. Jordà, M. Espino, and P. Marsaleix (2009a), Origin and dy-
634 namics of mesoscale eddies in the Catalan Sea (NW Mediterranean): Insight from

635 a numerical model study, *J. Geophys. Res.*, *114*(C06009), 0148–0227, doi:10.1029/
636 2007JC004245.

637 Rubio, A., B. Blanke, S. Speich, N. Grima, and C. Roy (2009b), Mesoscale eddy activity
638 in the southern Benguela upwelling system from satellite altimetry and model data,
639 *Prog. Oceanogr.*, *83*, 288–295.

640 Ruiz, S., J. Font, M. Emelianov, J. Isern-Fontanet, C. Millot, J. Salas, and I. Taupier-
641 Letage (2002), Deep structure of an open sea eddy in the Algerian Basin, *J. Mar. Sys.*,
642 *33-34*, 179–195, doi:10.1016/S0924-7963(02)00058-1.

643 Sammari, C., C. Millot, and L. Prieur (1995), Aspects of the seasonal and mesoscale vari-
644 abilities of the Northern Current inferred from the PROLIG-2 and PROS-6 experiments,
645 *Deep-Sea Res. I*, *42*, 893–917.

646 Schaeffer, J. (2010), Impact du vent sur la circulation hydrodynamique dans le Golfe du
647 Lion: modélisation haute résolution., Ph.D. thesis, Université du Sud Toulon-Var.

648 Signell, R., and W. Geyer (1991), Transient eddy formation around headlands, *J. Geophys.*
649 *Res.*, *96*(C2), 2561–2575.

650 Simpson, J. (1981), The Shelf-Sea Fronts: Implications of their Existence and Behaviour,
651 *Philosophical Transactions of the Royal Society of London. Series A, Mathematical and*
652 *Physical Sciences*, *302*(1472), 531–546.

653 Simpson, J., and D. Bowers (1981), Models of stratification and frontal movement in shelf
654 seas, *Deep-Sea Res. I*, *28*(7), 727 – 738, doi:DOI:10.1016/0198-0149(81)90132-1.

655 Trasvinã, A., E. D. Barton, J. Brown, H. S. Velez, P. M. Kosro, and R. L. Smith (1995),
656 Offshore wind forcing in the gulf of tehuantepec, mexico: The asymmetric circulation,
657 *J. Geophys. Res.*, *100*(20), 649–663, doi:10.1029/95JC01283.

Ulses, C., C. Estournel, J. Bonnin, X. Durrieu de Madron, and P. Marsaleix (2008a), Impact of storms and dense water cascading on shelf-slope exchanges in the Gulf of Lion (NW Mediterranean), *J. Geophys. Res.*, *113*, C02010, doi:10.1029/2006JC003795.

Ulses, C., C. Estournel, P. Puig, X. Durrieu de Madron, and P. Marsaleix (2008b), Dense shelf water cascading in the northwestern Mediterranean during the cold winter 2005: Quantification of the export through the Gulf of Lion and the Catalan margin, *Geophys. Res. Lett.*, *35*, L07610, doi:10.1029/2008GL033257.

Willett, C. S., R. R. Leben, and M. F. Lavín (2006), Eddies and Tropical Instability Waves in the eastern tropical Pacific: A review, *Prog. Oceanogr.*, *69*, 218–238, doi: 10.1016/j.pocean.2006.03.010.

Year	number of eddies	A1	lifetime days	A2	lifetime days
2001	1	23/07→06/10	76	-	-
2002	1	07/07→13/08	38	-	-
2003	2	07/07→18/08	43	12/09 →7/10	26
2004	0	-	-	-	-
2005	2	10/07→04/09	57	20/09 →04/10	15
2006	1	04/08→31/08	28	-	-
2007	0	-	-	-	-
2008	1	15/07→26/09	72	-	-

Table 1. Information on the long-life anticyclonic eddies present in the 2001-2008 modeling of the circulation in the western part of the GoL.

Year	2001	2002	2003	2004	2005	2006	2007	2008	8 years averaged
Percentage of NW wind (%)	55	59	50	53	53	47	62	54	54
Max. NW wind Amplitude(ms^{-1})	16	20	19	17	19	17	19	18	18
Avg. NW wind Amplitude (ms^{-1})	9	10	9	9	9	9	10	9	9

Table 2. Table of percentage of NW wind event and the corresponding maximum and average wind amplitude for the period May-October.

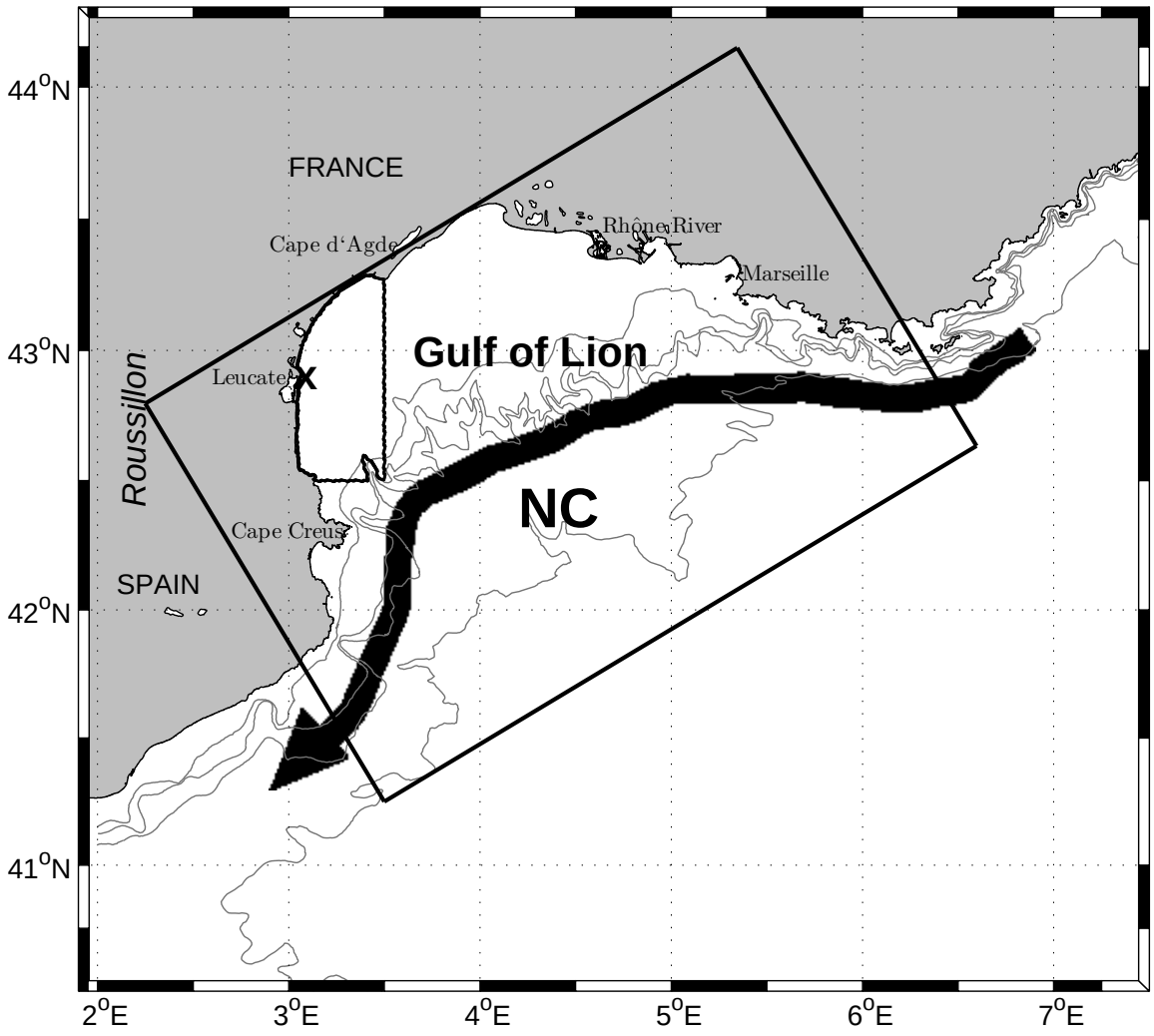

Figure 1. Map of the Gulf of Lion. The rectangle represents the model domain. The contour indicates the study area where eddies are often observed. The big cross indicates the location of meteorological station at Leucate. Isobaths at 100, 200, 500 and 2000 m are plotted with gray lines.

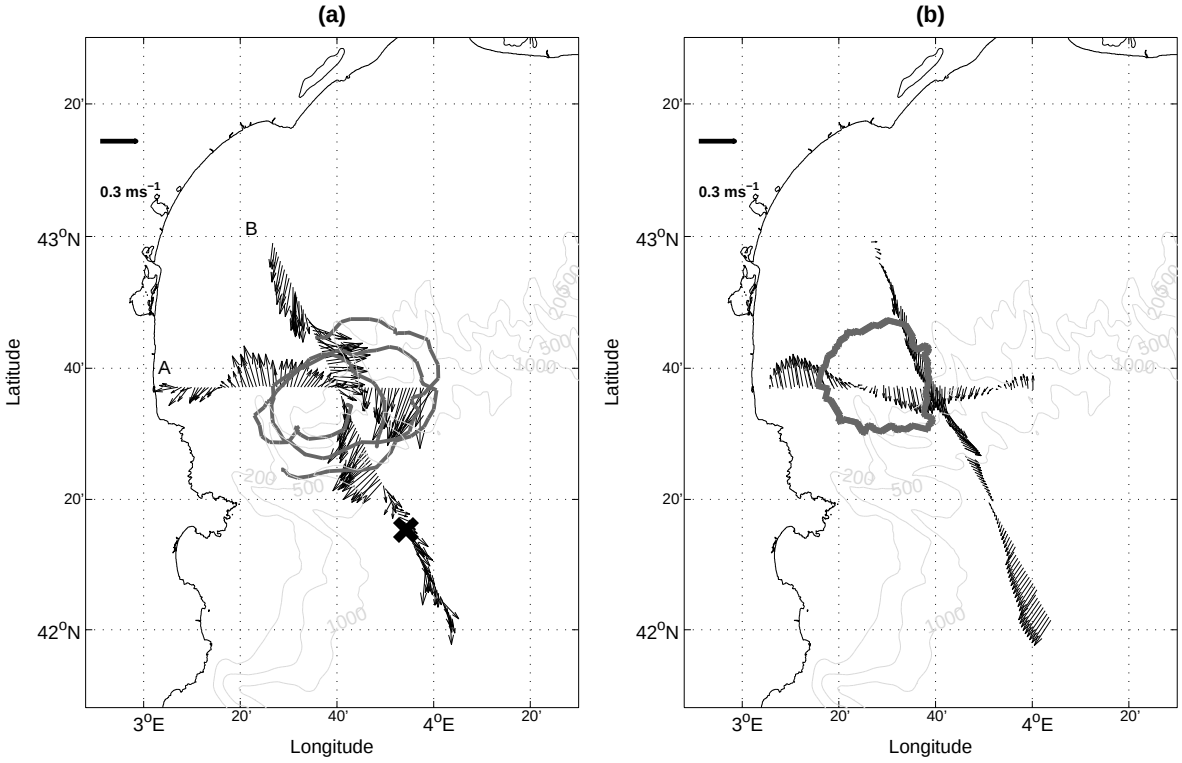

Figure 2. Comparison of the horizontal current field (ms^{-1}) at 15 m depth. a) ADCP measured current along transect A on Sept. 1, and along transect B on Sept. 5, 2008; dark gray contours represent the trajectories of two drifters from Sept. 5 to Sept. 11; the thick cross indicates XBT station; (b) simulated current averaged from 00:00 Sept. 1 to 00:00 Sept. 2 along transect A and from 00:00 Sept. 5 to 00:00 Sept. 6 along transect B; dark gray contour represent the eddy identification issued from the wavelet analysis on Sept. 10.

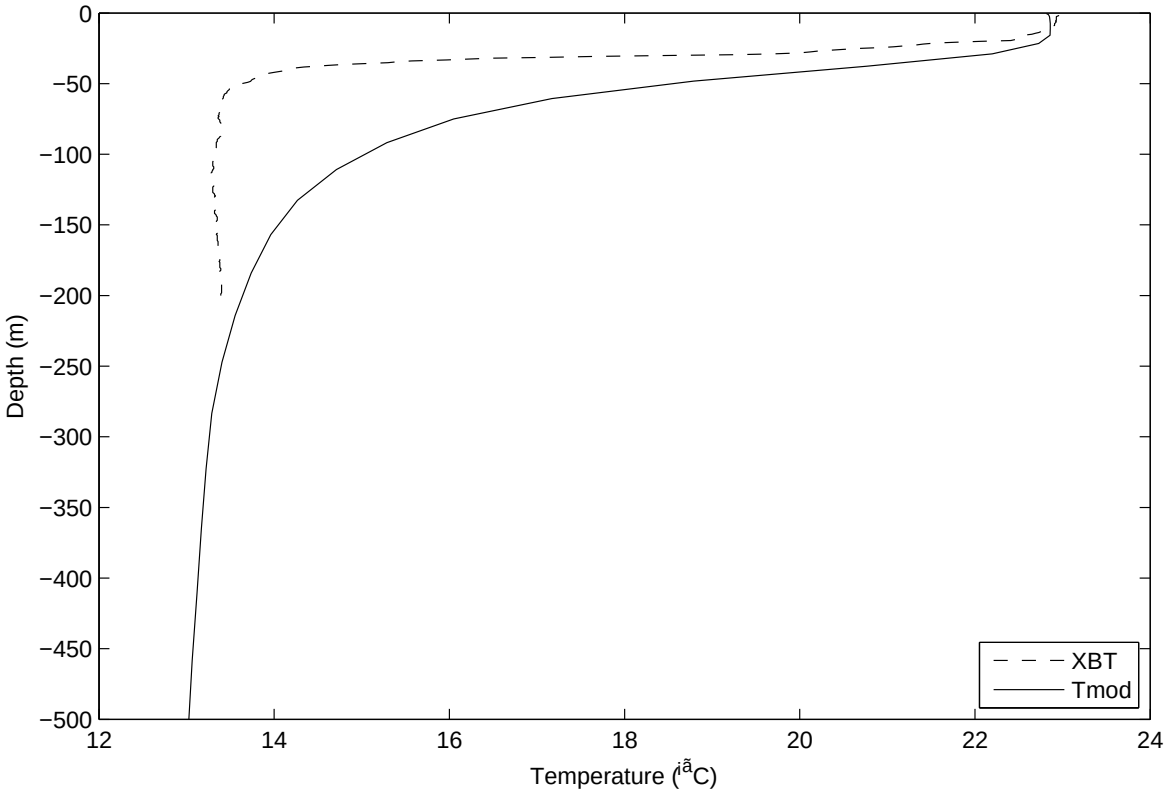

Figure 3. Vertical profile of temperature (°C) simulated (solid line) and measured (dashed line) by XBT at cross location in Fig.2.

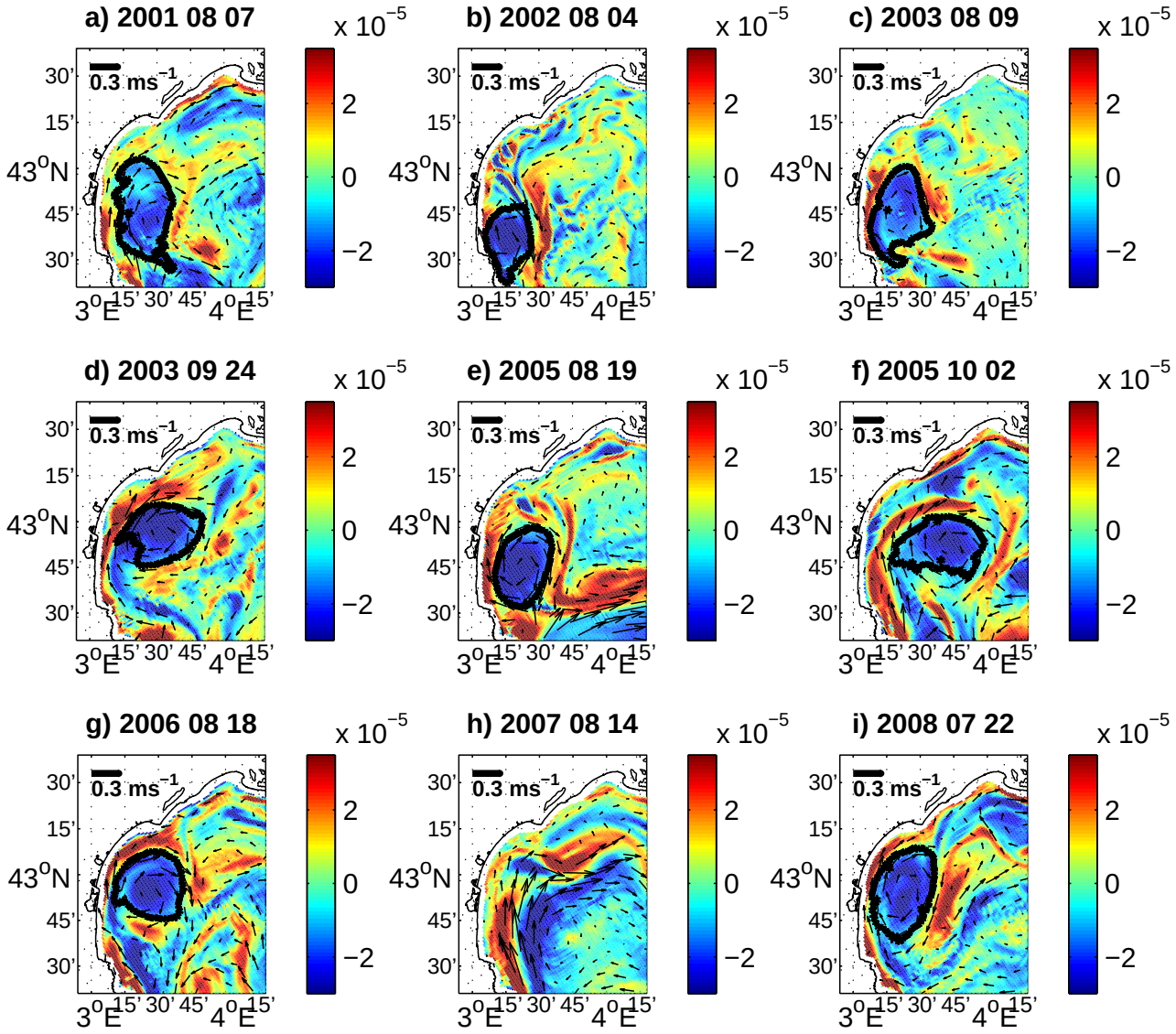

Figure 4. Snapshot of the modeled relative vorticity [s^{-1}] and current velocity at 20 m depth. The black contours issued from the wavelet analysis show the 8 long-life anticyclonic eddies once they are well-developed: a) A1_2001, b) A1_2002, c) A1_2003, d) A2_2003, e) A1_2005, f) A2_2005, g) A1_2006, i) A1_2008; and the circulation over the western part of the shelf is displayed in h).

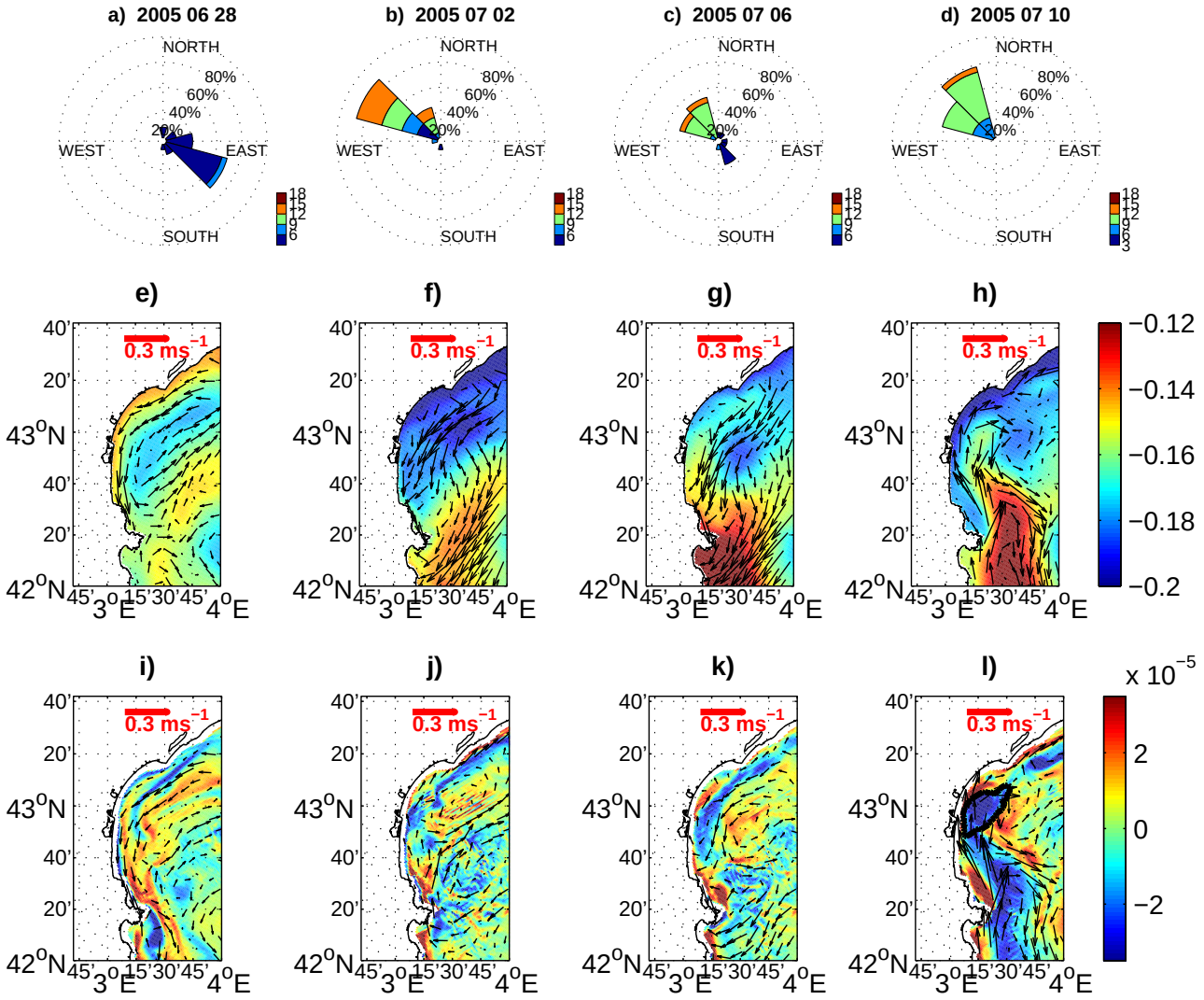

Figure 5. Time sequences of the generation process of the eddy A1_2005 with 4 days of interval. Top: wind rose representation (intensity and frequency) at station Leucate on a) 2005/06/26 to 28; b) 2005/06/30 to 07/02; c) 2005/07/04 to 06; d) 2005/07/08 to 10; colors representing wind intensity. Middle: sea surface height and current velocity field at 5 m depth on e) 2005/06/28; f) 2005/07/02; g) 2005/07/06; h) 2005/07/10. Bottom: relative vorticity (s^{-1}) computed at 20 m depth and current velocity fields corresponding to the same depth at the same dates as middle panels; black contour in l) shows the eddy identification issued from the wavelet analysis.

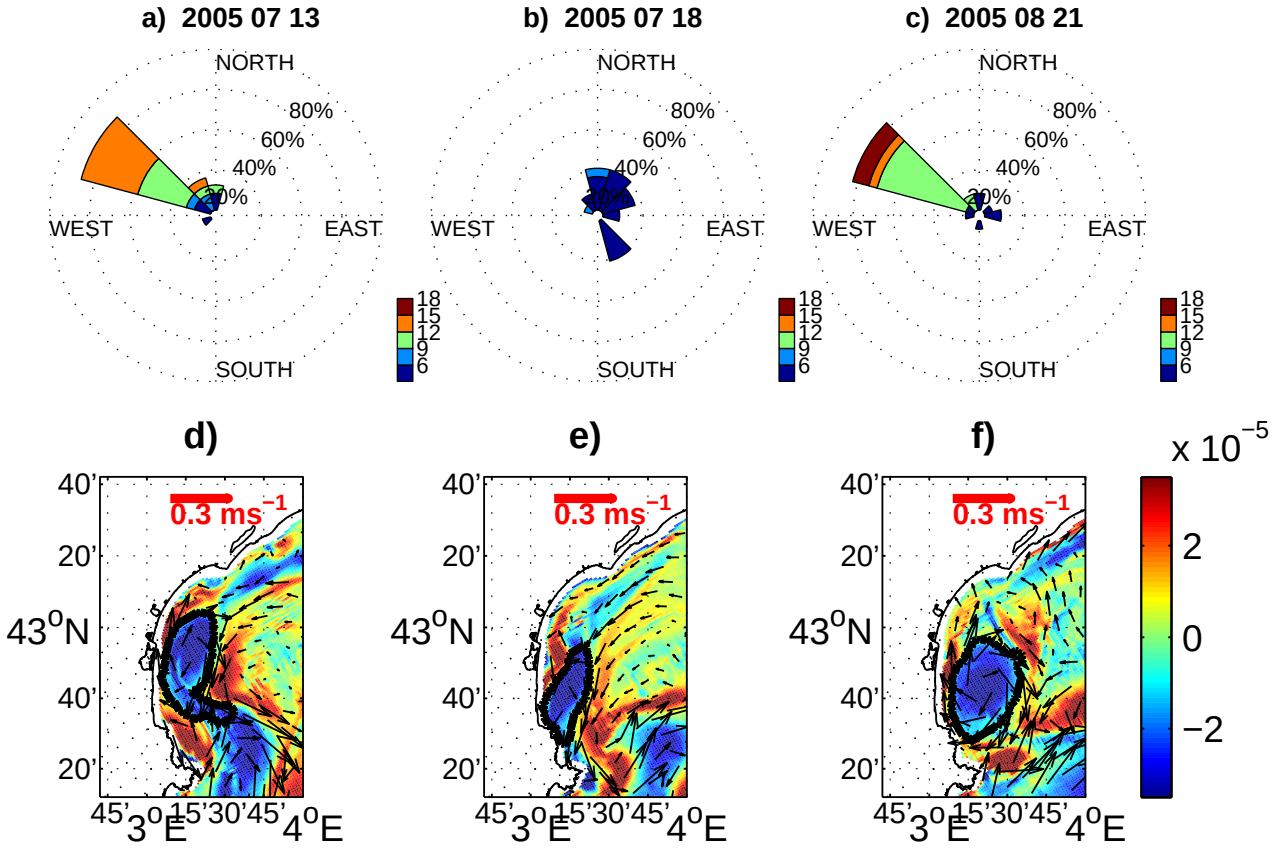

Figure 6. Time sequences of the evolution of the eddy A1_2005. Top: wind rose representation (intensity and frequency) at station Leucate on a) 2005/07/11 to 13; b) 2005/07/16 to 18; c) 2005/08/19 to 21; the location and extension of the fan sector indicating of a wind direction and its percentage; colors representing wind intensity. Bottom: relative vorticity (s^{-1}) computed at 20 m depth and current velocity fields corresponding to the same depth on d) 2005/07/13; e) 2005/07/18; f) 2005/08/21; black contours show the eddy identification issued from the wavelet analysis.

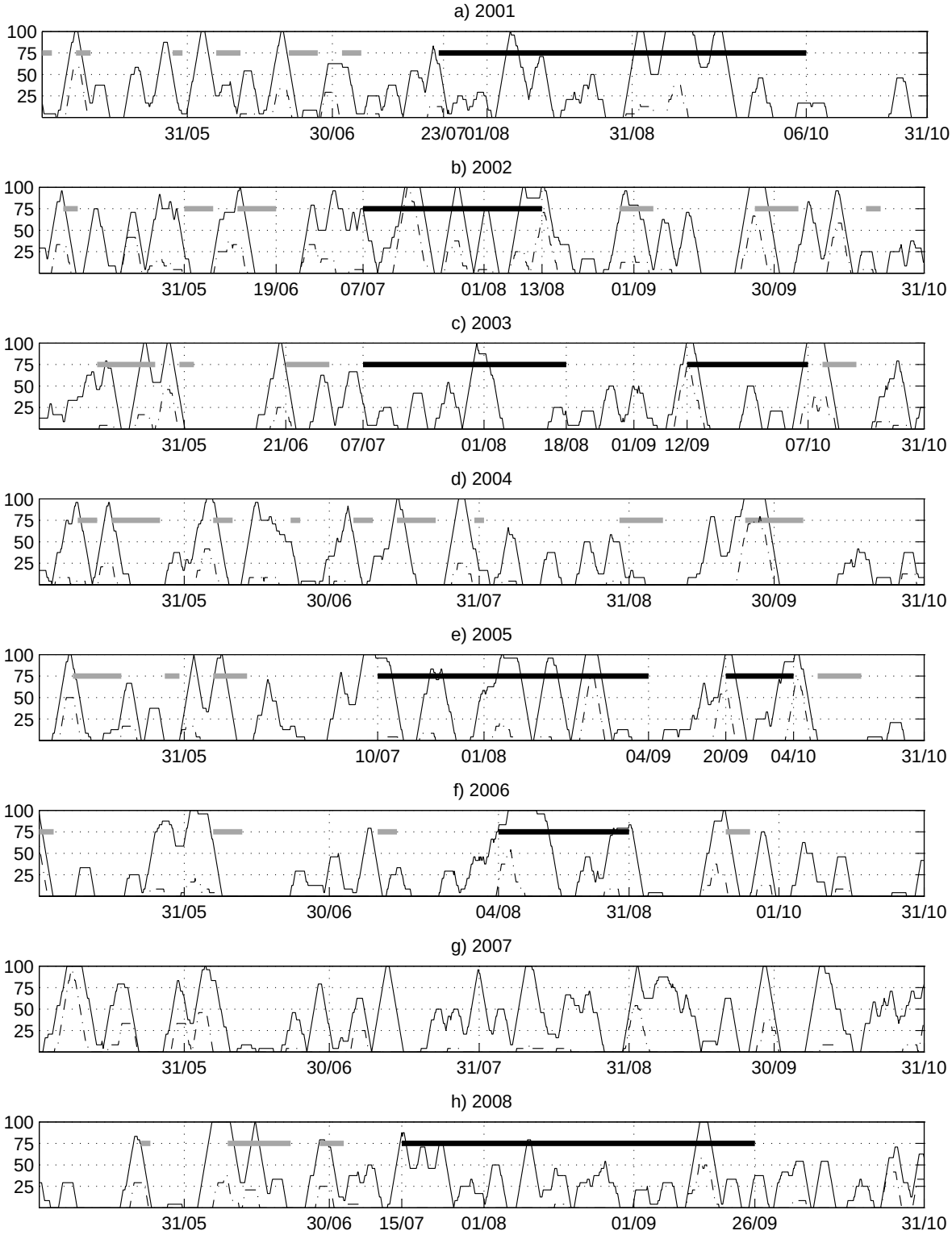

Figure 7. Temporal evolution of NW wind expressed as a percentage of all wind, with a 3 day moving average, (continuous line: NW wind intensity ≥ 8 ms^{-1}; dotted line: ≥ 14 ms^{-1}) from May 1 to October 31 for each year. The presence of 'long-life' eddies is indicated by a horizontal black thick line and the 'short-life' eddies' presence is indicated by a gray thick line.

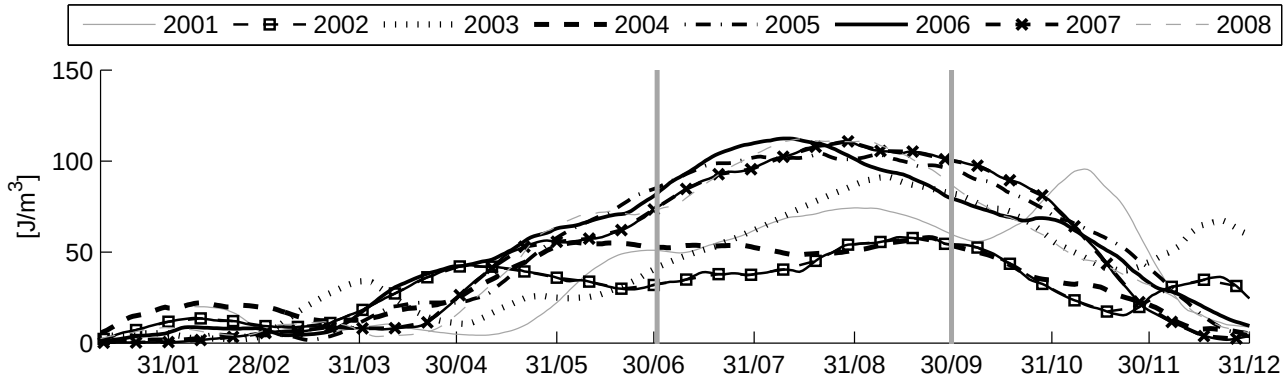

Figure 8. Time series of 30 day moving averaged potential energy anomaly [J/m^3] over the western part of the GoL for the upper 100 m depth for the years 2001-2008.

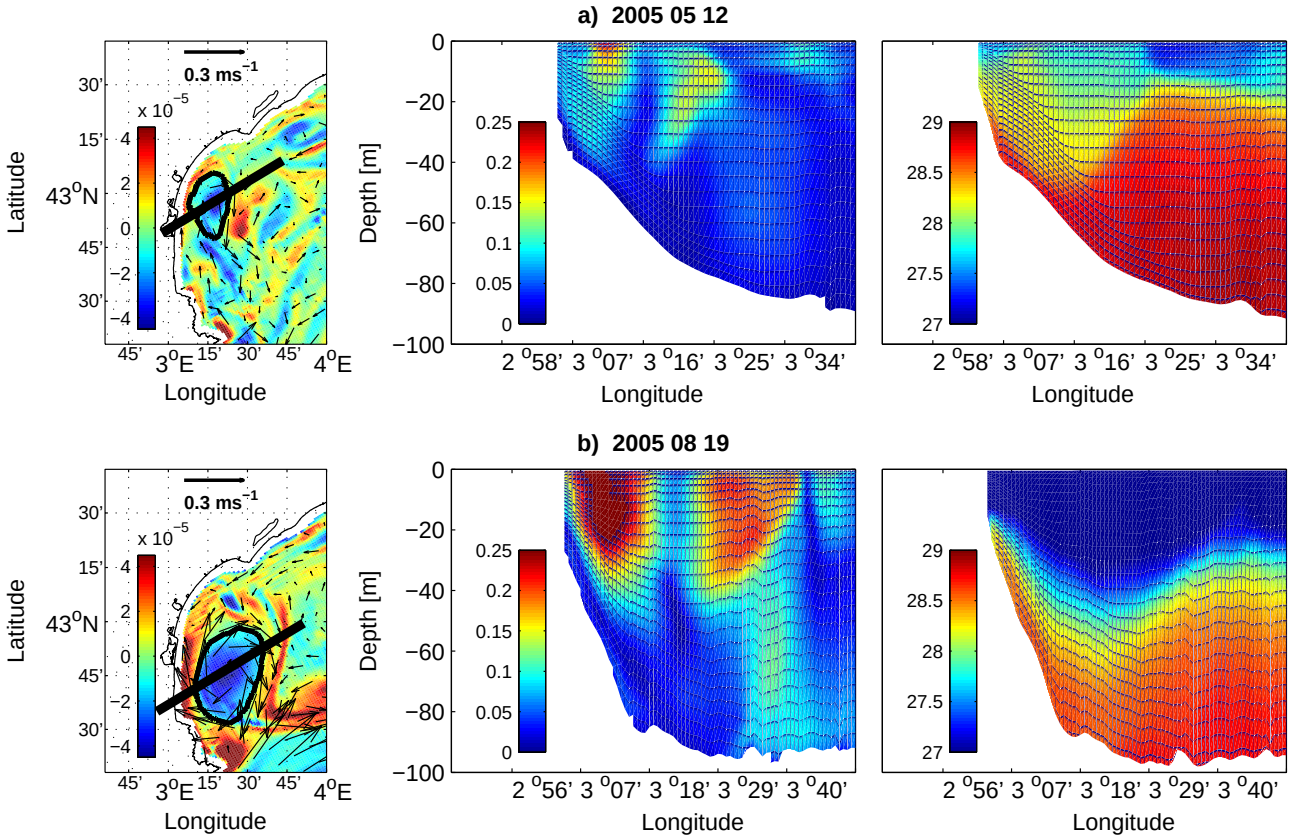

Figure 9. Left: relative vorticity at 20 m depth, current velocity fields and eddy contour; black line marks the eddy cross-section; Middle: Vertical transect of current intensity [ms^{-1}]; Right: Vertical transect of density for a): May 12 and b): August 19, in 2005.

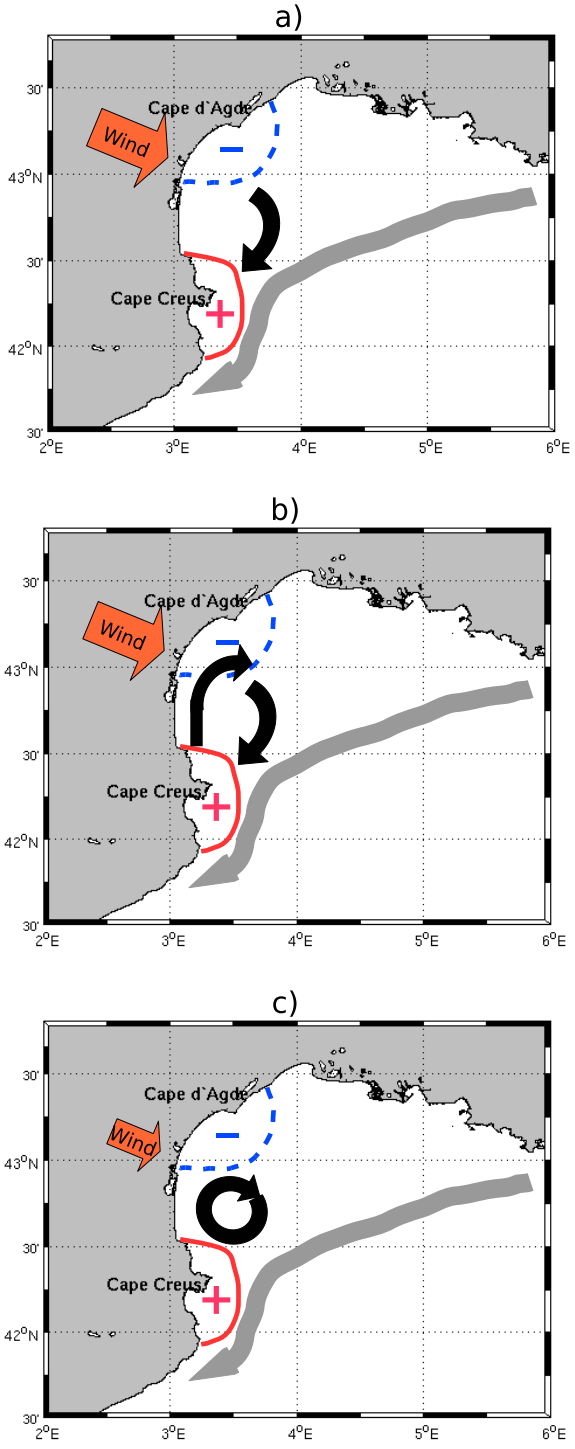

Figure 10. Schematic of anticyclonic eddy generation process. Wind forcing is indicated by the orange arrows; sea surface level (+/red or -/blue sign/zone); surface currents (black thick arrow); NC (gray thick line).